Plasma Chemistry and Plasma Processing (2020) 40:1365–1380
https://doi.org/10.1007/s11090-020-10097-9

ORIGINAL PAPER

Plasma Parameters and Silicon Etching Kinetics in $C_4F_8 + O_2 + Ar$ Gas Mixture: Effect of Component Mixing Ratios

Byung Jun Lee[1] · Alexander Efremov[2] · Yunho Nam[1] · Kwang-Ho Kwon[1]

Received: 8 April 2020 / Accepted: 4 June 2020 / Published online: 13 June 2020

Abstract
In this work, we investigated the possibidlxlity to control both gas-phase chemistry and silicon etching kinetics in $C_4F_8 + O_2 + Ar$ inductively coupled plasma by changes in O_2/Ar, C_4F_8/O_2 and C_4F_8/Ar mixing ratios at the constant fraction of the rest component (50%), gas pressure (10 mTorr), input power (700 W) and bias power (200 W). The combination of plasma diagnostics and modeling tools allowed one: (a) to compare the effects of gas mixing ratios on both steady-state plasma parameters and densities of active species; (b) to figure out key processes which determine the fluorine atom formation/decay balance in each gas system; and (c) to analyze the differences in Si etching kinetics in terms of process-condition-dependent effective reaction probability. It was shown that the maximum changes in gas-phase chemistry take place in O_2-rich plasmas due to $CF_x + O/O(^1D) \rightarrow CF_{x-1}O + F$, $CF_xO + e \rightarrow CF_{x-1}O + F + e$ and $CFO + O/O(^1D) \rightarrow CO_2 + F$ stepwise dissociation pathways. It was suggested also that the effective probability for $Si + xF \rightarrow SiF_x$ reaction may be controlled by either fluorocarbon film thickness (in C_4F_8—rich plasmas) or O atom flux (in Ar and O_2—rich plasmas) through the balance of adsorption sites on the etched surface.

Keywords C_4F_8-based plasma · Diagnostics · Modeling · Reaction kinetics · Etching · Polymerization

Introduction

Currently, the issue of global warming in the etching process is receiving attention. To reduce this global warming, conventional high global warming potential gases (CF_4, C_4F_8) are being replaced by liquified perfluorocarbon (L-PFC) precursor with low global warming potential. However, prior to the study of these L-PFC precursor, the etching mechanism of conventional fluorocarbon gas must be investigated. Fluorocarbon gases with a general

✉ Kwang-Ho Kwon
kwonkh@korea.ac.kr

[1] Department of Control and Instrumentation Engineering, Korea University, Sejong 30019, Republic of Korea

[2] Department of Electronic Devices and Materials Technology, State University of Chemistry and Technology, 7 Sheremetevsky av., Ivanovo, Russia 153000

formula of C_xF_y are widely used in the microelectronic industry for dry patterning of silicon and silicon-based materials—SiC, SiO_2 and Si_3N_4 [1–5]. Among these gases, only CF_4 provides the domination of etching over surface polymerization process (due to the domination of F atoms over CF_x radicals in a gas phase) and thus, works as a classical etchant. In a combination with the spontaneous $Si + xF \rightarrow SiF_x$ reaction, such feature provides high silicon etching rates, but results in both the nearly isotropic etching profile and the low SiO_2/Si etching rate ratio [1, 2]. Oppositely, the fluorocarbons with $y/x < 3$, such as C_2F_4, C_3F_6 and C_4F_8, exhibit high polymerization ability that causes lower Si etching rates together with the sufficient etching residues in a form of fluorocarbon polymer film. At the same time, these gases allow one to obtain the highly-anisotropic etching of silicon (due to the protection of side walls by the deposited fluorocarbon polymer layer) as well as the much higher SiO_2/Si etching rate ratio (due to the higher fluorocarbon film thickness on the oxygen-free surface) [3–5]. It is known also that the etching/polymerization balance in fluorocarbon-based plasmas may be effectively adjusted by the addition of Ar and/or O_2 in a feed gas [2, 5]. Corresponding mechanisms are connected with changes in both gas-phase (F atom yield, density and flux of polymerizing radicals) and heterogeneous (decomposition rate and thickness of the fluorocarbon polymer film) sub-systems. As such, the reasonable choice of the feed gas composition provides an additional tool to optimize the output etching process characteristics as well as the whole device performance.

Until now, there were several works dealt with investigations of both gas-phase chemistry and dry etching kinetics in C_4F_8-based plasmas [6–18]. The results of these works allowed one to figure out the processes which determine the densities of neutral and charged species in binary $C_4F_8 + Ar$ and $C_4F_8 + O_2$ gas mixtures [6–10], to find the phenomenological relationships between processing conditions, steady-state plasma parameters and etching kinetics of Si, SiO_2 and Si_3N_4 [11–15] as well as to compose reaction schemes providing an adequate description of plasma chemistry by plasma modeling [6–8, 16–18]. Based on these data, the most important features of given gas system may briefly be summarized as follows:

1. Under the low-pressure plasma conditions, both gas-phase and heterogeneous recombination of atoms and radicals does not reproduce the original C_4F_8 molecules. As a result, the latter appear to be completely dissociated while the dominant neutral species in bulk plasma are C_2F_4 and CF_x with $x = 1–3$ [6–8]. The stepwise formation of F atoms in electron-impact processes as well as by their effective loss in gas-phase reactions provide the condition of $n_F \ll n_{CF_x}$ [9, 10]. At the same time, the absolute F atom density in pure C_4F_8 plasma is quite close to that in CF_4 under one and the same operating conditions [16, 19].
2. In most of cases, the deposited fluorocarbon polymer film is thick enough to limit the transport of F atoms to the film/treated surface interface [11, 12]. That is why the etching kinetics of Si, SiO_2 and Si_3N_4 in C_4F_8-based plasmas strongly depends on the thickness of polymer layer [13–15] that influences both effective reaction probability and etching yield [15, 17]. The addition of O_2 reduces the polymer film thickness and returns the etching process to the "normal" regime where the etching rate is controlled by F atom and/or ion fluxes [11, 13, 14].
3. The variations of component mixing ratios in both $C_4F_8 + Ar$ and $C_4F_8 + O_2$ gas systems lead to similar non-monotonic changes in both Si and SiO_2 etching rates [11, 13, 14]. According to Ref. [16], the transition toward O_2-rich $C_4F_8 + O_2$ gas mixtures does not result in increasing F atom density, as it was repeatedly mentioned for $CF_4 + O_2$ [5,

20, 21]. As such, the effects of non-monotonic etching rates were always attributed to changes in fluorocarbon polymer thickness [11–14].

In our opinion, there are at least two principal problems that may play a critical role for the etching process optimization. First, the really insufficient attention was paid to plasma chemistry and etching kinetics in the three-component $C_4F_8+O_2+Ar$ gas mixtures, and particularly to the effect of gas mixing ratios. At the same time, our previous works [16, 22] clearly demonstrated that (a) the variations in O_2/Ar and CF_4/O_2 mixing ratios in the qualitatively similar CF_4+O_2+Ar gas system provide the wide-range adjustment of densities and fluxes of plasma active species due to changes in both electro-physical plasma parameters (electron temperature, electron density, ion bombardment energy) and gas-phase reaction kinetics; and (b) the impact of O_2/Ar mixing ratio on the properties of CF_4+O_2+Ar and $C_4F_8+O_2+Ar$ plasmas under one and the same operating conditions is quite different. And secondly, the interpretations of experimental data on both plasma parameters and etching kinetics in most of cases were not matched with the plasma chemistry analysis. Therefore, since the basic relationships between gas-phase and heterogeneous sub-systems were not clearly understood, some uncertainties in conclusions on etching mechanisms took place. For example, Refs. [11, 14] attributed the non-monotonic (with maximum at ~ 50% of additive gas) Si and SiO_2 etching rates in C_4F_8+Ar and $C_4F_8+O_2$ plasmas to the change in the fluorocarbon film thickness. At the same time, this formally contradicts with monotonic change in measured film thickness as well as with the maximum on the corresponding dependence of the polymer deposition rate [11]. As such, the detailed study of both gas-phase and heterogeneous phenomena in $C_4F_8+O_2+Ar$ mixture is an important task for enriching fundamental knowledge on fluorocarbon gas plasma chemistry, for understanding etching mechanisms and thus, for future progress in dry etching technology.

The idea of this work was to apply the previously developed research scheme (the combination plasma diagnostics by Langmuir probes and 0-dimensional plasma modeling [16–18]) to study the $C_4F_8+O_2+Ar$ inductively coupled plasma in three different gas mixing regimes which assume changes in O_2/Ar, C_4F_8/O_2 and C_4F_8/Ar mixing ratios at constant fraction the third component. The questions of primary attention were a) to demonstrate the ability of $C_4F_8+O_2+Ar$ gas system to adjust the plasma parameters and composition using the gas mixing ratios only; b) to determine the gas mixing effects on parameters which directly influence the heterogeneous reaction kinetics (fluxes of active species and flux-to-flux ratios characterizing the etching/polymerization balance); and c) to analyze the features of Si etching mechanism in terms of process-condition-dependent effective reaction probability.

Experimental and Modeling Details

Experimental Setup and Procedures

Both plasma diagnostics and etching experiments were performed in the planar inductively coupled plasma (ICP) reactor, the same as that used in our previous studies [16–18]. Plasma was excited using the 13.56 MHz power supply connected to the copper coil at the top of the chamber. Another 12.56 MHz rf generator biased the bottom electrode which was used as a holder for etched samples. The fixed bias power W_{dc}

corresponded to the variable negative dc bias voltage $-U_{dc}$. Also, the bottom electrode had a built-in water-flow cooling system that allowed one to maintain its constant temperatures T_S during the etching process.

Plasma parameters were examined by the double Langmuir probe tool DLP2000 (Plasmart Inc.) that provided the information on electron temperature (T_e) and saturated ion current density (J_+). In order to minimize experimental errors due to the deposition of fluorocarbon polymer on probe tips, latter were cleaned in 50% Ar + 50% O_2 plasma before and after each measurements. Our previous studies [16, 18] have demonstrated the efficiency of such cleaning procedure to extract an adequate diagnostics data. The total positive ion density n_+ was found from $J_+ \approx 0.61 e n_+ v_B$ assuming the collision-less transport of ions through probe sheath [5, 23]. The expression for ion Bohm velocity $v_B \approx \sqrt{eT_e/m_i}$ neglected the impact of negative ions. From previously published works [16, 22, 24], it can be understood that such simplification is quite applicable to low-pressure electronegative plasmas. The variable (i.e. the dependent on the initial mixture composition) effective ion mass was determined as $m_i = (\sum y_{X_i^+}/m_{X_i^+})^{-1}$, where $m_{X_i^+}$ and $y_{X_i^+}$ are individual ion masses and fractions inside n_+. Parameters $y_{X_i^+}$ were estimated assuming their proportionality to $k_{iz} y_X / \sqrt{1/m_{X^+}}$, where k_{iz} is the ionization rate coefficient [7, 8], and y_X is the fraction of corresponding neutral particle.

Silicon etching kinetics was studied using the fragments of Si wafer with dimensions of about 2 × 2 cm which were placed in the middle part of the bottom electrode. The small sample size allowed one to neglect the loading effect as well as to provide the etching regime controlled by heterogeneous process kinetics. In preliminary experiments, it was found that there are no principal (i.e. exceeding the standard experimental error) differences in Langmuir probe diagnostics results with and without etched samples in the reactor chamber. In fact, such situation allows one to neglect feedbacks between heterogeneous and bulk subsystems as well as to assume the gas-phase as the steady-state source of active species when analyzing the plasma-surface interaction effects. Silicon etching rates were determined from corresponding etched depths Δh measured by a surface profiler (Alpha-step 500, Tencor) for a processing time of $\tau = 60$ s. Since the condition $\tau < 300$ s surely provided the steady-state etching regime (that follows from the quasi-linear $\Delta h = f(\tau)$ curves), one can simply accept $R = \Delta h/\tau$. The experiments indicated also that there are no principal differences in Si etching kinetics for samples placed in different radial positions on the bottom electrode. This allows one to assume the spatially independent etching mechanism, and the weakly decreasing absolute etching rates toward chamber walls may be associated with the non-uniform radial profiles of densities and fluxes of plasma active species [5].

In order to examine the effects of various component mixing ratios, we conducted three experimental series where the initial $C_4F_8 + O_2 + Ar$ gas compositions were set by adjusting the partial flow rates for mixture components—$q_{C_4F_8}$, q_{O_2} and q_{Ar}. The constant parameters were total gas flow rate ($q = 40$ sccm), gas pressure ($p = 10$ mTorr), input power ($W = 700$ W), bias power ($W_{dc} = 200$ W) and etched sample temperature ($T_S \sim 17$ °C). In first experimental series, the fraction of C_4F_8 ($y_{C_4F_8} = q_{C_4F_8}/q$) was fixed at 50%, and the variable parameters were y_{O_2} and y_{Ar}. An increase in y_{O_2} from 0 to 50% corresponded to the transition from 50% C_4F_8 + 50% Ar to 50% C_4F_8 + 50% O_2 gas system. In second experimental series, we changed the fractions of C_4F_8 and O_2 at constant $y_{Ar} = 50\%$. As such, an increase in y_{O_2} from 0 to 50% corresponded to the transition from 50% C_4F_8 + 50% Ar to 50% O_2 + 50% Ar gas system. Accordingly, in third experimental series variable parameters were $y_{C_4F_8}$ and y_{Ar} at constant y_{O_2}. An increase in y_{Ar} from 0 to 50% corresponded to the transition from 50% C_4F_8 + 50% O_2 to 50% O_2 + 50% Ar gas system. For convenience,

the information of gas mixing regimes corresponding to various experimental series is summarized in Table 1.

Plasma Modeling

In order to obtain the densities and fluxes of plasma active species, we used a simplified zero-dimensional kinetic model with the experimental data on T_e and n_+ as input parameters [16–18, 24]. The basic kinetic scheme (the set of reactions with corresponding rate coefficients) for $C_4F_8+O_2+Ar$ gas system was taken from our previous work [16, 17]. In order to provide the more accurate description of gas-phase reactions involving O and $O(^1D)$ species, we took into account their formation and decay mechanisms with a participation of $O_2(a^1\Delta)$ and $O_2(b^1\Sigma)$ molecules [25, 26]. The modeling algorithm was built in using the standard approaches for low pressure ($p<50$ mTorr) electronegative plasmas, including the fluorocarbon-based gas systems. Particularly, it was assumed that:

1. The electron energy distribution function (EEDF) has the nearly Maxwellian shape. The applicability of Maxwellian EEDFs to describe electron-impact kinetics in low-pressure C_4F_8-based plasmas has been demonstrated in several works [6–8, 16, 27] by the acceptable agreement between the experimental and modeling data. This allows one to obtain the electron-impact rate coefficients from the fitting expressions in a form of $k = AT_e^B\exp\left(-C/T_e\right)$, where coefficients A, B and C are available from published works [7, 27].
2. The low electronegativity of $C_4F_8+O_2+Ar$ plasma under the given set of processing conditions provides $n_-/n_e \ll 1$ and $n_e \approx n_+$, where n_e and n_- are densities of electrons and negative ions, respectively [6, 16, 17]. As such, one may limit the kinetic scheme by neutral species only as well as may not account for the influence of dissociative attachment processes on plasma parameters and active species kinetics.
3. The dependence of gas temperature on component mixing ratios at $p, W=$const may be ignored. Accordingly, the condition $T_{gas} \approx$ const allows one to operate with the constant rate coefficients for gas-phase atom-molecular reactions.
4. The heterogeneous decay of unsaturated ground-sate (C_xF_y, F, C, O) and excited ($O(^1D)$, $O_2(a^1\Delta)$, $O_2(b^1\Sigma)$, $Ar(^3P_{0,1,2})$) species is described by the conventional first-order recombination kinetics. Corresponding recombination probabilities may be taken from Refs. [7, 16, 17] where these were either obtained experimentally or adjusted by modeling procedure to obtain the agreement between measured and model-predicted species densities.

Table 1 Gas mixing regimes in various experimental series

No. exp.	Component fractions in $C_4F_8+O_2+Ar$ (%)								
	Mixing regime 1			Mixing regime 2			Mixing regime 3		
	$y_{C_4F_8}$	y_{O_2}	y_{Ar}	$y_{C_4F_8}$	y_{O_2}	y_{Ar}	$y_{C_4F_8}$	y_{O_2}	y_{Ar}
1.	50	0	50	50	0	50	50	50	0
2.	50	12	38	38	12	50	38	50	12
3.	50	25	25	25	25	50	25	50	25
4.	50	38	12	12	38	50	12	50	38
5.	50	50	0	0	50	50	0	50	50

The output model parameters were the volume-averaged steady-state densities of plasma active species and their fluxes to the etched surface. More details on modeling assumptions, algorithms, computational procedures and sources of chemical kinetics data may be found in Refs. [16–18].

Results and Discussion

When analyzing the plasma chemistry in the multi-component gas mixture, the question of primary importance is how the mixing ratios of various feed gas components do influence the gas-phase plasma characteristics. The key issues here are the electrons-related parameters (electron temperature, electron density) that determine formation rates of plasma active species in electron impact processes (and thus, their densities and fluxes to the treated surface) as well as the ions-related parameters (ion flux and ion energy on the plasma sheath edge) characterizing the intensity of ion bombardment. From Fig. 1, one can conclude that the investigated gas mixing regimes provide different and sometimes opposite effects on the kinetics of both electron-impact reactions and ion-assisted heterogeneous processes. The obtained results may be summarized as follows:

- The substitution of Ar for O_2 at $y_{C_4F_8}$ = const lowers both electron temperature (4.3–3.2 eV for 0–50% O_2, Fig. 1a) and densities of charged species (5.0×10^{10}–3.9×10^{10} cm^{-3} for 0–50% O_2, Fig. 1b). A decrease in T_e may surely be associated with higher electron energy losses in the low-threshold excitation of O_2 and other molecular reaction products (FO, CF_xO, CO, CO_2 [16]) compared with those for Ar atoms. It should be noted that such situation is quite typical for binary mixtures of noble and molecular gases. The decreasing tendency for n_+ (and thus, for n_e when assuming the quasi-neutrality condition in a form of $n_e \approx n_+$) may result from the simultaneous decrease in total ionization rate and an increase in loss rates for both electrons and positive ions. The first phenomenon takes place because of both lower rate coefficients for R1: $O_2 + e \rightarrow O_2^+ + 2e$ ($k_1 \sim 1.3\times10^{-10}$ cm^3 s^{-1} for $T_e = 3$ eV) and R2: $O + e \rightarrow O^+ + 2e$ ($k_2 \sim 2.1\times10^{-10}$ cm^3 s^{-1} for $T_e = 3$ eV) compared with R3: $Ar + e \rightarrow Ar^+ + 2e$ ($k_3 \sim 2.6\times10^{-10}$ cm^3 s^{-1} for $T_e = 3$ eV) and a fall of ionization efficiency together with T_e (for example, 7.5×10^{-10}–2.1×10^{-10} cm^3 s^{-1} for k_1 and 1.7×10^{-9}–3.6×10^{-10} cm^3 s^{-1} for k_3 at 0–50% O_2). The second mechanism probably works through increasing rates of dissociative attachment and ion-ion recombination due to increasing densities of electronegative oxygen-containing species. The total flux of positive ions Γ_+ follows the behavior of n_+ and change from 8.5×10^{15}–6.1×10^{15} cm^{-2} s^{-1} for 0–50% O_2. The weakly increasing $-U_{dc}$ (298–332 V for 0–50% O_2, Fig. 1c) and ion bombardment energy $\varepsilon_i \approx e\left|-U_f - U_{dc}\right|$, where U_f is the floating potential, does not compensate for the fall of Γ_+. As a result, the parameter $\sqrt{M_i\varepsilon_i}\Gamma_+$ characterizing the ion momentum flux [16, 18, 22] also demonstrates the monotonic fall toward higher y_{O_2} values (1.1×10^{18}–7.7×10^{17} $eV^{1/2}$ cm^{-2} s^{-1} for 0–50% O_2, Fig. 1d). Therefore, the given gas mixing regime suppresses electron-impact kinetics (due to a simultaneous decrease in T_e and n_e) as well as lowers the intensity of ion bombardment.
- The substitution of C_4F_8 for O_2 at y_{Ar} = const also results in decreasing T_e (4.3–3.6 eV for 0–50% O_2, Fig. 1a), but causes a weak growth in densities of charged species (5.0×10^{10}–6.3×10^{10} cm^{-3} for 0–50% O_2, Fig. 1b). Obviously, the similar (in respect to the previous mixing regime) influence of C_4F_8/O_2 mixing ratio on electron temper-

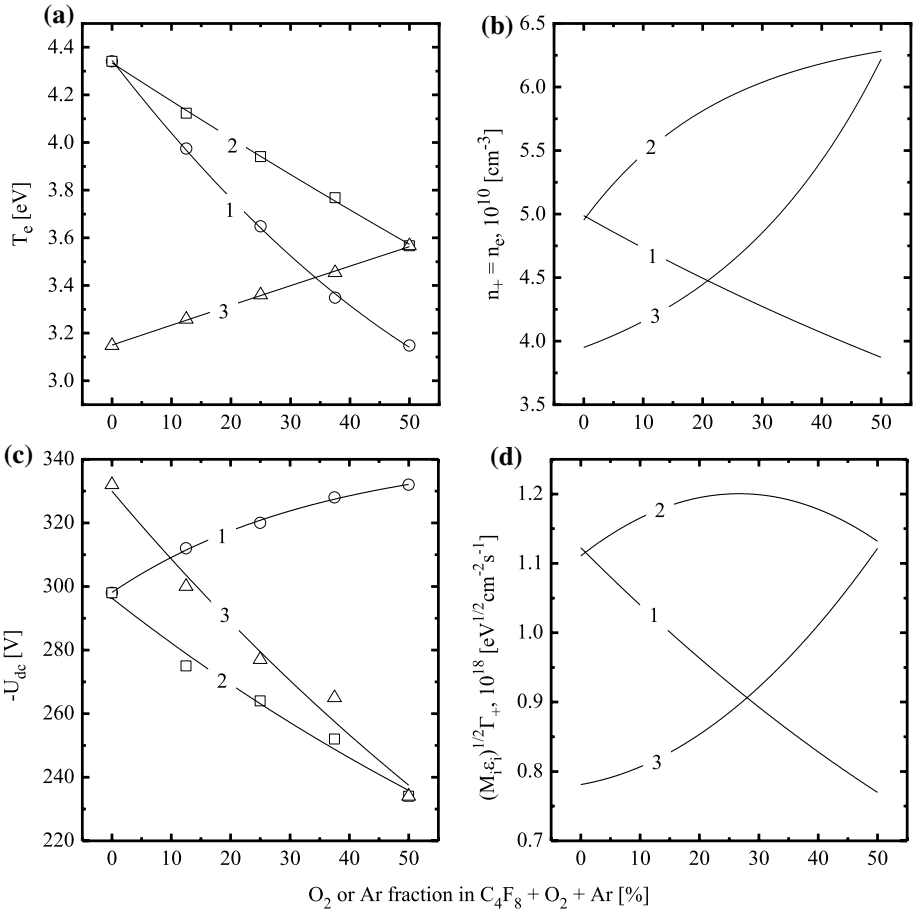

Fig. 1 Electron temperature (**a**), densities of charges species (**b**), negative dc bias (**c**) and the parameter $\sqrt{M_i\varepsilon_i}\Gamma_+$ characterizing ion momentum flux (**d**) as functions of component mixing ratios in $C_4F_8+O_2+Ar$ gas mixture. Numbers on curves relate to different gas mixing regimes (see Table 1). The corresponding "x" axis arguments are: 1—y_{O_2} (the substitution of Ar for O_2) at constant fraction of C_4F_8; 2—y_{O_2} (the substitution of C_4F_8 for O_2) at constant fraction of Ar; and 3—y_{Ar} (the substitution of C_4F_8 for Ar) at constant fraction of O_2

ature results from the similar change in EEDF which reduces the high-energy "tail" with increasing O_2 fraction in a feed gas. The reason is the wider range of electron energy losses for O_2 molecules compared with CF_x species provided by the low-threshold processes R4: $O_2+e\rightarrow O_2(a^1\Delta)+e$ ($\varepsilon_{th}\sim 1.0$ eV) and R5: $O_2+e\rightarrow O_2(b^1\Sigma)+e$ ($\varepsilon_{th}\sim 1.6$ eV). An increase in both n_+ and n_e results from the combination of nearly constant total ionization rate and decreasing heterogeneous loss rates for electrons and positive ions. The first phenomenon takes place because a bit lower rate coefficient for R1 compared with R6: $CF_x+e\rightarrow CF_x^+ +2e$ ($k_6\sim 1.5\times 10^{-10}$ cm^3 s^{-1} for x = 1, $\sim 3.5\times 10^{-10}$ cm^3 s^{-1} for x = 2 and $\sim 1.3\times 10^{-10}$ cm^3 s^{-1} for x = 3 at T_e = 3 eV) is compensated by a) high dissociation degree for O_2 molecules that provides $n_O \approx n_{O_2}$ with $k_2 > k_1$; and b) contributions of R7: $O_2(a^1\Delta)+e\rightarrow O_2^+ +2e$ ($k_7\sim 4.7\times 10^{-10}$ cm^3 s^{-1} at T_e = 3 eV), R8: $O_2(b^1\Sigma)+e\rightarrow O_2^+ +2e$ ($k_8\sim 5.5\times 10^{-10}$ cm^3 s^{-1} at T_e = 3 eV) and R9:

$O(^1D) + e \rightarrow O^+ + 2e$ ($k_9 \sim 5.8 \times 10^{-10}$ cm^3 s^{-1} at $T_e = 3$ eV). The mentioned changes in the heterogeneous loss kinetics follow from the decreasing T_e that lowers both effective diffusion coefficient for electrons and ion Bohm velocity. The change of Γ_+ (8.5×10^{15}–1.2×10^{16} cm^{-2}s^{-1} for 0–50% O_2) meets the opposite tendency of ion bombardment energy due to a decrease in $-U_{dc}$ (298–234 V for 0–50% O_2, Fig. 1c). As a result, the parameter $\sqrt{M_i \varepsilon_i} \Gamma_+$ keeps the nearly constant value of about 1.2×10^{17} eV$^{1/2}$cm^{-2} s^{-1} (Fig. 1d). Therefore, the given gas mixing regime does not produce principal changes in both electron-impact kinetics (due to the opposite changes in T_e and n_e) and ion bombardment intensity.

- The substitution of C_4F_8 for Ar at $y_{O_2} = \text{const}$ accelerates the electron-impact kinetics through increasing tendencies for both T_e (3.2–3.6 eV for 0–50% Ar, Fig. 1a) and densities of charged species (3.9×10^{10}–6.3×10^{10} cm^{-3} for 0–50% Ar, Fig. 1b). The behavior of T_e has the similar nature with that mentioned for the first gas mixing regime. Really, as the electron-impact excitation processes for Ar atoms are characterized by higher threshold energies and lower cross-section compared with those for CF_x species, an increase in y_{Ar} reduces the electron energy losses in the middle part of EEDF and thus, increases the amount electrons with higher energies. The growth of n_+ and n_e may surely be associated with an increase in total ionization rate. The reasons are that a) the absolute values of k_3 and the particle-type-averaged k_6 are quite close; b) k_3 is more sensitive to an increase in T_e due to the higher threshold energy for R3 (~ 15.6 eV) compared with R6 (~ 10 eV); and c) the ionization rate in Ar-rich plasmas is contributed by R10: $Ar(^3P_{0,1,2}) + e \rightarrow Ar^+ + 2e$ ($k_{10} \sim 8.4 \times 10^{-8}$ cm^3 s^{-1} at $T_e = 3$ eV). In contrast to the previous case, an increase in Γ_+ (6.1×10^{15}–1.2×10^{16} cm^{-2} s^{-1} for 0–50% Ar) appears to be stronger compared with a decrease in both $-U_{dc}$ (332–234 V for 0–50% O_2, Fig. 1c) and ion bombardment energy. As such, the change in $\sqrt{M_i \varepsilon_i} \Gamma_+$ (7.7×10^{17}–1.1×10^{18} eV$^{1/2}$cm^{-2} s^{-1} for 0–50% Ar, Fig. 1d) points out on increasing ion bombardment intensity.

Among the neutral gas-phase components, the species of primary interest are F atoms (as etchants for treated surface), fluorocarbon radicals CF_x with x = 1 and 2 (as polymerizing species providing the formation of the fluorocarbon polymer film on the plasma/surface interface) and O atoms (as etchants for the fluorocarbon polymer film). From modeling results, it was found that the given set of operating conditions provides all typical features mentioned in previous works [6–9, 16–18, 28]. These are:

1. The dominant species in the non-oxygenated $C_4F_8 + Ar$ gas system are C_2F_x (x = 3, 4) and CF_x (x = 1, 2, 3) radicals while the densities of F and F_2 are lower by about an order of magnitude. In this group, only C_2F_4 and CF_2 are the first-step dissociation products of original C_4F_8 molecules which appear in R11: $C_4F_8 + e \rightarrow C_3F_6 + CF_2 + e$ and R12: $C_4F_8 + e \rightarrow 2C_2F_4 + e$. The condition $n_{CF_2} > n_{C_2F_4}$ (~ 9.2×10^{13} cm^{-3} и ~ 3.4×10^{13} cm^{-3}, respectively, for 50% C_4F_8 + 50% Ar gas system) is provided by R13: $C_2F_4 + e \rightarrow 2CF_2 + e$, R14: $C_2F_4 + e \rightarrow C_2F_3 + F + e$ and R15: $C_2F_4 + F \rightarrow CF_2 + CF_3$.
2. The main source of F atoms is R16: $CF_x + e \rightarrow CF_{x-1} + F + e$ (x = 1–3) while the dominant decay mechanisms for these species are a group of heterogeneous processes R17: $CF_x + F \rightarrow CF_{x+1}$ together with R15. Since the latter exceeds R17 by about an order of magnitude, the condition $n_{CF_x} > n_F$ always takes place. Accordingly, the impact from R18: $F_2 + e \rightarrow 2F + e$ to the total F atom formation rate does not exceed 1% due to $n_{CF_x} \gg n_{F_2}$.

3. The addition of O_2 introduces new reaction pathway for both fluorocarbon species and oxygen-containing products. The most effective ones are R19: $CF_x + O/O(^1D) \rightarrow CF_{x-1}O + F$, R20: $CFO + O/O(^1D) \rightarrow CO_2 + F$, R21: $FO + O/O(^1D) \rightarrow O_2 + F$ and R22: $CF_xO + e \rightarrow CF_{x-1}O + F + e$. In general case (i.e. without accounting for the specific gas mixing regime), the related effects provide an increase in decomposition rate for CF_x radicals, the limitation of gas-phase densities of CF_xO and FO compounds as well as increasing formation rates for F, CO and CO_2.

Figures 2 and 3 illustrate the effects of various gas mixing regimes on densities and kinetics of selected neutral species. The substitution of Ar for O_2 at $y_{C_4F_8}$ = const lowers the efficiency of R16 (for example, $k_{16}n_e$ = 59–24 s^{-1} for CF_3 and 95–31 s^{-1} for CF_2 at 0–50% O_2) as well as limits the rates of R23: $O_2 + e \rightarrow 2O + e$, R24: $O_2 + e \rightarrow O + O(^1D) + e$ and R25: $O + e \rightarrow O(^1D) + e$ because of the fast decay of O_2 molecules in R26: $CF + O_2 \rightarrow CFO + O$ ($k_{26} \sim 3.2 \times 10^{-11}$ cm^3 s^{-1}) and R27: $C + O_2 \rightarrow CO + O$ ($k_{27} \sim 1.6 \times 10^{-11}$ cm^3 s^{-1}). As a result, the lack of oxygen atoms ($n_O = 4.3 \times 10^{10}$–2.2×10^{11} cm^{-3} for 12–50%

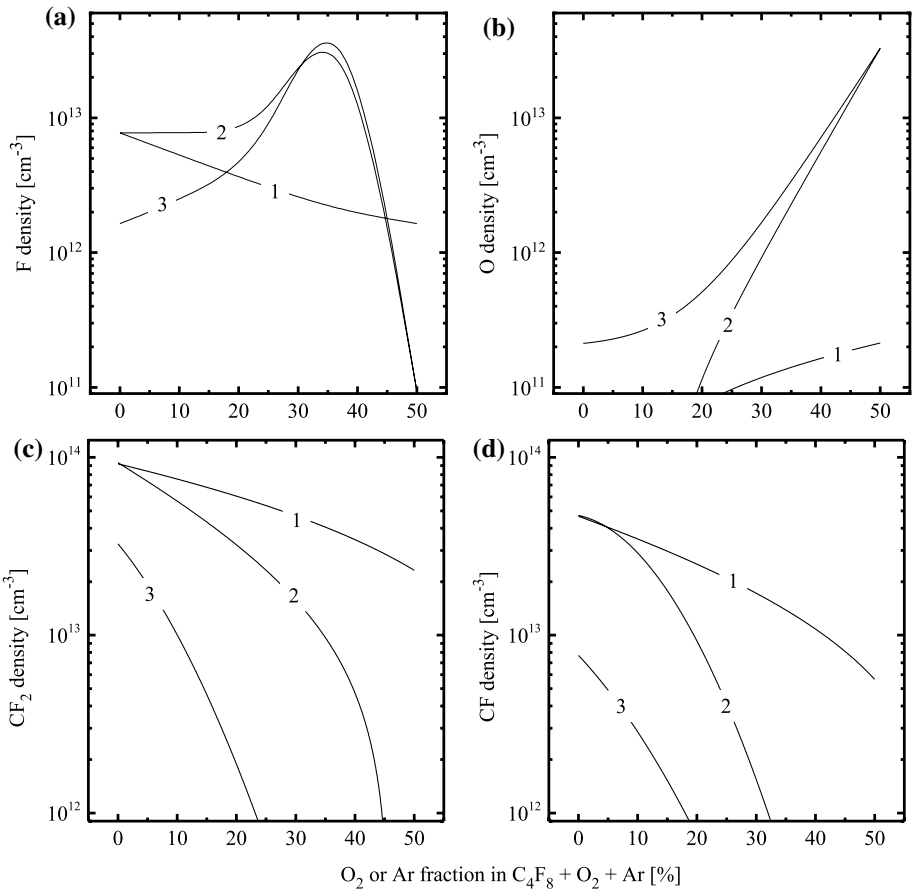

Fig. 2 Densities of selected neutral species as functions of component mixing ratios in $C_4F_8 + O_2 + Ar$ gas mixture. Numbers on curves relate to different gas mixing regimes and "x" axis arguments, as in Fig. 1

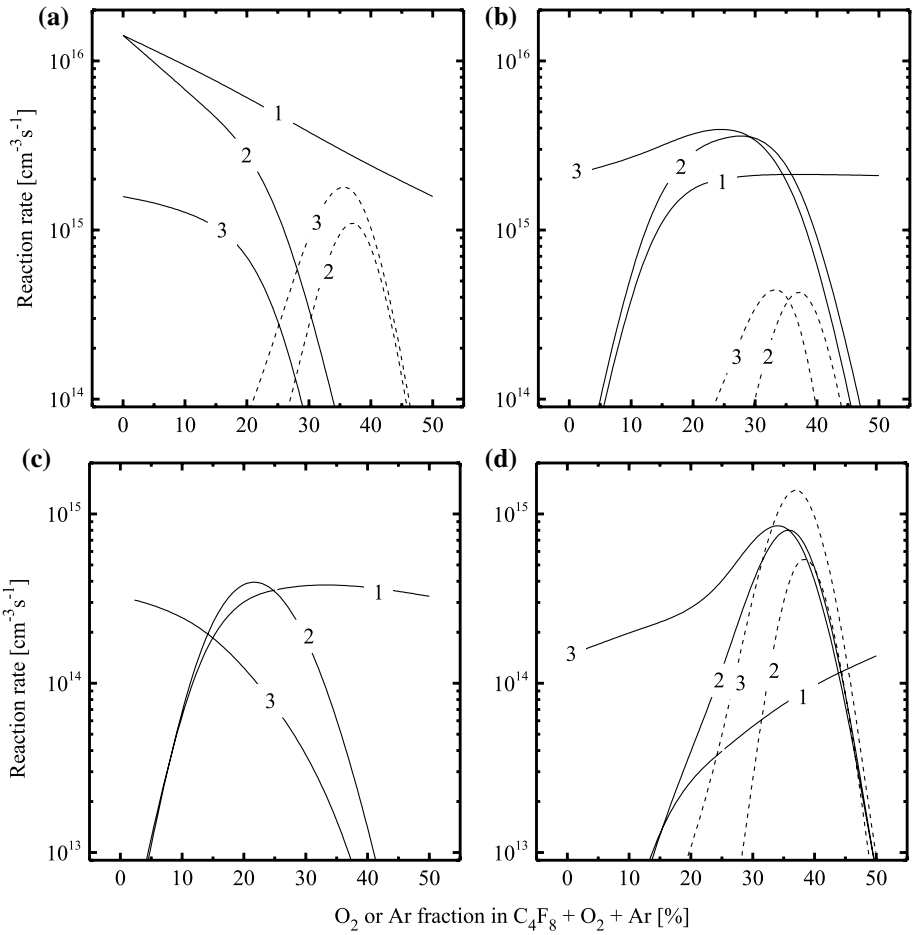

Fig. 3 Fluorine atom formation rates through different reaction pathways as functions of component mixing ratios in $C_4F_8+O_2+Ar$ gas mixture. **a** $CF_x+e\rightarrow CF_{x-1}+F+e$ (solid lines) and $F_2+e\rightarrow 2F+e$ (dashed lines). **b** $CF_xO+e\rightarrow CF_{x-1}O+F+e$ (solid lines) and $FO+e\rightarrow F+O+e$ (dashed lines). **c** $CF_x+O/O(^1D)\rightarrow CF_{x-1}O+F$. **d** $CFO+O/O(^1D)\rightarrow CO_2+F$ (solid lines) and $FO+O/O(^1D)\rightarrow O_2+F$ (dashed lines). Numbers on curves relate to different gas mixing regimes and "x" axis arguments, as in Fig. 1

O_2, Fig. 2d) provides the condition $R_{16}>\sum_{i=19}^{22}R_i$ (Fig. 3) even for the 50% $C_4F_8+50\%$ O_2 gas mixture. Accordingly, the transition toward O_2-rich plasmas is accompanied by monotonically decreasing densities for both F atoms (by ~ 5 times, see Fig. 2a) and polymerizing radicals (by ~ 4 times for CF_2 and by ~ 8 times for CF, see Fig. 2b, c).

The substitution of C_4F_8 for O_2 at $y_{Ar}=$ const lowers the amount of fluorocarbon component in a feed gas and thus, suppresses both the formation of F atoms in R16 (1.3×10^{16}–1.4×10^{13} cm^{-3} s^{-1}, or by ~ 900 times for 0–38% O_2, see Fig. 3a) and the loss of O_2 molecules through R26 and R27. The last effect causes the much faster increase in O_2, O and O(^{1}D) densities compared with previous case (Fig. 2d), creates the favorable conditions for R19–R22 and provides the noticeable contribution of these processes to the

total F atom formation rate starting from $y_{O_2} \sim 25\%$ (Fig. 3). Accordingly, the range of 0–40% O_2 is featured by the deep fall in densities of CF_x radicals (by ~ 450 times for CF_3, by ~ 1000 times for CF_2 and by ~ 500 times for CF at 0–38% O_2, see Fig. 2b, c) as well as by the condition $R_{16} + \sum_{i=19}^{22} R_i \approx$ const. Simultaneously, the decreasing density of C_2F_4 (by more than three orders of magnitude, owing to R28: $C_2F_4 + O/O(^1D) \rightarrow CF_2O + CF_2$) suppresses R15 and thus, reduces the effective (i.e. composed by the net effect from R15 and R17) decay frequency for F atoms by ~ 25 times, from 1500 to 60 s^{-1} for 0–38% O_2. All these result in the non-monotonic (with a maximum at ~ 35–40% O_2, see Fig. 2a) dependence of F atom density on y_{O_2}.

The substitution of C_4F_8 for Ar at $y_{O_2} = \text{const}$ increases the efficiency of R16 (for example, $k_{16}n_e = 24$–38 s^{-1} for CF_3 and 31–72 s^{-1} for CF_2 at 0–50% Ar) as well as always fits the conditions $y_{O_2} > y_{C_4F_8}$. An excess of O and $O(^1D)$ species in a gas phase (Fig. 2b) rapidly transfers the CF_x radicals in a form of CF_xO and FO compounds (Fig. 2c, d) as well as provides an increase in $\sum_{i=19}^{22} R_i$ up to 35–40% Ar mostly owing to R20, R21 and R22 (Fig. 3). As a result, the total F atom formation rate $R_{16} + \sum_{i=19}^{22} R_i$ exhibits a maximum at ~ 35 to 40% Ar. In addition, the rapid consumption of C_2F_4 in R28 lowers the effective decay frequency for F atoms in similar extent as was mentioned for the previous case (1220–60 s^{-1}, or by ~ 20 times for 0–38% Ar). All these provide the stronger (in respect to the initial F atom density) maximum on the $n_F = f(y_{Ar})$ curve (Fig. 2a).

Summarizing above data, one should mention that the effect of component mixing ratios on the chemistry of neutral species (in fact, on the chemical etching pathway) is much stronger compared with the change in ion bombardment intensity. It is also clear that only two gas mixing regimes are able to provide the effective adjustment for the etching/polymerization balance through the opposite changes in densities of F atoms and polymerizing radicals. At the same time, the qualitatively similar behaviors in F atom density obtained in second and third gas mixing regimes (particularly, an increase in n_F in the range of 0–35% O_2 or Ar) are caused by different mechanisms. These are either the change in F atom decay kinetics at constant formation rate or an increase in formation rate together with the change in decay kinetics. One can suggest that the first case may be more sensitive to reactor chamber materials through the recombination probability for F atoms.

Figure 4 shows the influence of gas mixing regimes on silicon etching kinetics. For the interpretation of these data, one can account for known features of the reactive-ion etching process in polymerizing plasmas [5, 13, 15, 29–33]:

1. The measured etching rate, R_{Si}, may be represented in a form of two summands, $R_{phys} + R_{chem}$. The first summand is the rate of physical sputtering given by $Y_S \Gamma_+$ [29], where $Y_S \sim \sqrt{M_i \varepsilon_i}$ [22, 24] is the Si sputtering yield. The second summand is the rate of ion-assisted reaction $Si + xF \rightarrow SiF_x$ which may be found as $\gamma_R \Gamma_F$. The effective reaction probability γ_R decreases with increasing thickness of the fluorocarbon polymer film as well as depends on any factor influencing the fraction of free adsorption sites for F atoms.
2. The growth of the fluorocarbon polymer film is provided by the CF_x (x = 1, 2) radicals, and the polymerization ability increases in fluorine-poor plasmas [15, 32]. Accordingly, the polymer deposition rate may be traced by the Γ_{pol}/Γ_F ratio [22, 33], where $\Gamma_{pol} = \Gamma_{CF_2} + \Gamma_{CF}$, and the parameters $\Gamma_{pol}/\sqrt{M_i \varepsilon_i}\Gamma_+ \Gamma_F$ and $\Gamma_{pol}/\Gamma_O \Gamma_F$ characterize the change in the polymer film thickness, h_{pol}, due to physical (sputtering by ion bombardment) and chemical (etching by O atoms) destruction pathways [16, 33].

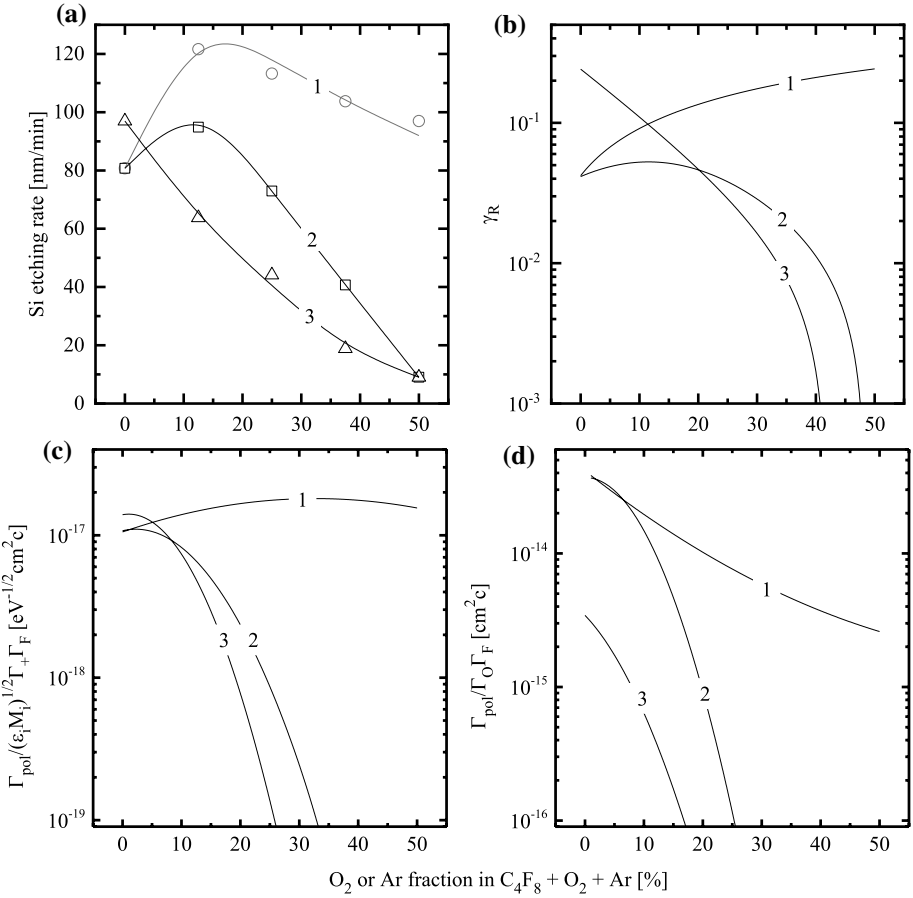

Fig. 4 Silicon etching kinetics (**a**, **b**) and parameters characterizing the decomposition of fluorocarbon polymer film by physical (**c**) and chemical (**d**) pathways as functions of component mixing ratios in $C_4F_8+O_2+$Ar gas mixture. Numbers on curves relate to different gas mixing regimes and "x" axis arguments, as in Fig. 1

From Fig. 4a, it can be seen that the substitution of Ar for O_2 at $y_{C_4F_8}=$const causes the non-monotonic behavior of Si etching rate. Particularly, the latter increases from 81 to 122 nm min^{-1} up to 10–15% O_2 and then shows a smooth fall in more oxygenated plasmas reaching 97 nm min^{-1} at 50% O_2. At the same time, the etching rate in the fluorineless plasma is much lower and does not exceed 10 nm min^{-1} even for higher $\sqrt{M_i\varepsilon_i}\Gamma_+$ values. This allows one to conclude that a) the given set of operating conditions provide $R_{phys} \ll R_{chem}$; and b) the mentioned non-monotonic change in R_{Si} is completely associated with R_{chem}. The change in effective reaction probability $\gamma_R = R_{Si}/\Gamma_F$ (0.043–0.24 for 0–50% O_2, Fig. 4b) contradicts with the behavior of $\sqrt{M_i\varepsilon_i}\Gamma_+$, but demonstrates an agreement with decreasing polymer film thickness. The last conclusion directly follows from the combination of nearly constant $\Gamma_{pol}/\sqrt{M_i\varepsilon_i}\Gamma_+\Gamma_F$ (Fig. 4c) and decreasing $\Gamma_{pol}/\Gamma_O\Gamma_F$ (Fig. 4d) that points out on the shift in the polymer formation/destruction balance toward the destruction. Similar correlations (the lower polymer film thickness, the higher reaction probability or etching yield) have been reported in several experimental works [13, 15, 34]

for Si, SiO_2, and Si_3N_4. As such, one can surely suggest that the non-monotonic Si etching rate is produced by the opposite changes in F atom flux and effective reaction probability while an increase in γ_R results from decreasing h_{pol} that promotes the transport of F toms to the etched surface [5, 13–15].

The substitution of C_4F_8 for O_2 at y_{Ar} = const lowers also results in non-monotonic $R_{Si} = f\left(y_{O_2}\right)$ curve with a quite similar position in etching maximum etching rate. Compared with previous case, the main differences are the weaker etching rate growth in the pre-maximum region (81–95 nm min^{-1} for 0–50% O_2) as well as the deeper fall down to the value of ~ 9 nm min^{-1} provided by the physical sputtering only (Fig. 4a). The effective reaction probability shown in Fig. 4b keeps the nearly constant value for 0–25% O_2 and then shows the fast decrease with increasing y_{O_2}. At the same time, the data of Fig. 4c, d indicate the deep fall of both $\Gamma_{pol}/\sqrt{M_i\varepsilon_i}\Gamma_+\Gamma_F$ and $\Gamma_{pol}/\Gamma_O\Gamma_F$ values that may be associated with the rapidly decreasing h_{pol}. As such, the given gas mixing regime provides no agreement in change of γ_R and h_{pol}, as was mentioned in previous case. Based on this fact, one can suggest that under the condition of $y_{C_4F_8} < y_{O_2}$ the Si etching kinetics is much less affected by the polymer deposition/destruction balance due to the low h_{pol} value. In our opinion, the nearly constant γ_R in the range of 0–25% O_2 is associated with the same behaviors of $\sqrt{M_i\varepsilon_i}\Gamma_+$ and surface temperature (i.e. with nearly constant fraction of free adsorption sites for F atoms) while a decrease in effective reaction probability in more oxygenated plasmas may be connected with two mechanism. First mechanism is the oxidation of reaction products into SiF_xO_y compounds which may exhibit lower volatility compared with SiF_x. Though this suggestion cannot be confirmed directly by experimental data, one can refer for similar differences in volatilities of non-oxidized and oxidized silicon chlorides and bromides [35, 36]. And secondly, one can simply imagine that an increasing flux of O atoms passivate the surface through their chemisorption and formation of Si–O bonds. Obviously, this lowers the amount of adsorption sites for F atoms as well as increases the overall reaction threshold.

The substitution of C_4F_8 for Ar at y_{O_2} = const causes the monotonic decrease in both Si etching rate (97–9 nm min^{-1} for 0–25% Ar, Fig. 4a) and effective reaction probability (Fig. 4b). Since an increase in Ar mixing ratio always corresponds to $y_{C_4F_8} < y_{O_2}$ as well as leads to the deep fall of h_{pol} (as follows from the changes in $\Gamma_{pol}/\sqrt{M_i\varepsilon_i}\Gamma_+\Gamma_F$ and $\Gamma_{pol}/\Gamma_O\Gamma_F$ in Fig. 4c, d) the situation looks to be quite similar to the previous case. One should mention only that the 50% C_4F_8 + 50% O_2 plasma, as the starting point in this gas mixing regime, provides the lower amount of deposited fluorocarbon polymer (or even the polymer-free surface) together with the higher O atom flux. Probably, this causes the stronger impact of oxygen-flux-related effects Si etching kinetics as well as results in higher sensitivity of γ_R to the change in Γ_O.

Another possible mechanism which may influence γ_R in given gas system is the defluorination of polymer film by ion bombardment. Particularly, Standaert et al. [15] has demonstrated that the ion-induced generation of F atoms within the polymer layer impacts the Si etching kinetics together with the polymer film thickness. However, this conclusion was made for the case of very thick (~ 100 nm) polymer film which was especially deposited before the etching. Obviously, the thick film retards the access of F atoms from a gas phase to Si surface, and the F atoms produced by the polymer itself may play the noticeable role in the etching process. At the same time, Ref. [15] reported also that the steady-state h_{pol} on silicon treated in pure C_4F_8 plasma under quite close to our case operating conditions is about few monolayers, or ~ 1 to 2 nm. Since our experiments were always performed with the half-diluted C_4F_8 gas and in the presence of oxygen, the similar or even lower h_{pol} may reasonably be assumed. Accordingly, such

situation provides the much easier access of F atoms from a gas phase trough the polymer film as well as the much lower contribution of F atoms generated in the polymer layer. From Ref. [15], it can be understood also that the change in defluorination degree may be traced by the parameter $\sqrt{M_i\varepsilon_i}\Gamma_+$, as was suggested for any ion-induced process. The rater weak changes of $\sqrt{M_i\varepsilon_i}\Gamma_+$ in all three gas mixing regimes (Fig. 1d) indicate that, even if the defluorination contributes γ_R, it works as a nearly constant summand. Moreover, in all there cases the behavior of γ_R (Fig. 4b) contradicts with that for $\sqrt{M_i\varepsilon_i}\Gamma_+$ (Fig. 1d), and thus, with the defluorination degree. All these suggest that, under the given set of processing conditions, the polymer defluorination effect is not a critical issue determining the silicon etching kinetics.

From above data, one can surely conclude that the influence of each gas mixing regime on Si etching kinetics is not controlled by the F atom flux only, but also assumes the change in the effective reaction probability. The nature of last effect depends on $y_{C_4F_8}/y_{O_2}$ ratio through either the deposition/destruction balance for the fluorocarbon polymer film or the oxygen-induced heterogeneous processes on the polymer-free surface. Particularly, under the condition of $y_{C_4F_8}/y_{O_2} > 1$ (in fact, under the combination of high flux for polymerizing radicals and low flux of oxygen atoms), the polymer film is thick enough to influence γ_R through the transport of F atoms to the etched surface. As such, the typical rule "the thicker polymer film, the lower reaction probability" does work. The condition $y_{C_4F_8}/y_{O_2} < 1$ provides the polymer-pure surface, but also limits γ_R through decreasing fraction of adsorption sited for F atoms. The suggested mechanisms are the oxidation of reaction product to the lower volatile compounds as $SiF_x + yO \rightarrow SiF_xO_y$ or the concurrent adsorption of O atoms with the formation of Si–O bonds. Obviously, all these provide the reasonable explanation of experimental results, but require additional investigations in the field of heterogeneous chemistry analysis.

Conclusions

In this work, we investigated how various gas mixing regimes in the three-component $C_4F_8 + O_2 + Ar$ gas system (the change in O_2/Ar mixing ratio at constant fraction of C_4F_8, the change in C_4F_8/O_2 mixing ratio at constant fraction of Ar and the change in C_4F_8/Ar mixing ratio at constant fraction of O_2) do influence on plasma parameters, densities of active species and silicon etching kinetics. From the plasma chemistry analysis, it was found that (a) all three component ratios affect the electron-impact kinetics through changes in both electron density and temperature; (b) the O_2-rich gas mixtures provide the noticeable changes in gas-phase reaction kinetics due to $CF_x + O/O(^1D) \rightarrow CF_{x-1}O + F$, $CF_xO + e \rightarrow CF_{x-1}O + F + e$ and $CFO + O/O(^1D) \rightarrow CO_2 + F$ stepwise dissociation pathways; and c) the variations in C_4F_8/O_2 and C_4F_8/Ar mixing ratios result in non-monotonic (with a maximum at ~ 35% Ar or O_2) behaviors of F atom density. In the case of C_4F_8/O_2 mixing, the last effect is not connected with an increase in total F atom formation rate, but is caused by the decrease in their loss rate in $C_2F_4 + F \rightarrow CF_2 + CF_3$. The analysis of Si etching kinetics with model-predicted fluxes of active species allowed one to suggest that the effective probability for the heterogeneous Si + F reaction may be sensitive to different factors, depending on the C_4F_8 fraction in a feed gas. This may be either the fluorocarbon film thickness (in C_4F_8—rich plasmas) or the balance of adsorption sites for F atoms on the polymer-free surface (in Ar and O_2—rich plasmas).

Acknowledgements The work was supported by the Korea Institute of Energy Technology Evaluation and Planning (KETEP) and the Ministry of Trade, Industry & Energy (MOTIE) of the Republic of Korea (No. 20172010105910) (B. J. Lee, Y. Nam and K.-H. Kwon).

References

1. Sugano T (1985) Applications of plasma processes to VLSI technology. Wiley, New York
2. Tauber RN, Wolf S (2000) Silicon processing for the VLSI erall. Process Technology, vol 1. Lattice Press, New York
3. Roth JR (1995) Industrial plasma engineering. Institute of Physics Publishing, Philadelphia
4. Adams AC, Sze SM (1988) VLSI technology. McGraw-Hill, New York
5. Lieberman MA, Lichtenberg AJ (2005) Principles of plasma discharges and materials processing. Wiley, New York
6. Rauf S, Ventzek PL (2002) Model for an inductively coupled Ar/c-C_4F_8 plasma discharge. J Vac Sci Technol A 20(1):14–23
7. Kokkoris G, Goodyear A, Cooke M, Gogolides E (2008) A global model for C_4F_8 plasmas coupling gas phase and wall surface reaction kinetics. J Phys D Appl Phys 41(19):195211
8. Vasenkov AV, Li X, Oehrlein GS, Kushner MJ (2004) Properties of c-C_4F_8 inductively coupled plasmas. II. Plasma chemistry and reaction mechanism for modeling of Ar/c-C_4F_8/O_2 discharges. J Vac Sci Technol A 22(3):511–530
9. Zhao SX, Zhang YR, Gao F, Wang YN, Bogaerts A (2015) Bulk plasma fragmentation in a C_4F_8 inductively coupled plasma: a hybrid modeling study. J Appl Phys 117(24):243303
10. Kazumi H, Hamasaki R, Tago K (1996) Model prediction of radical composition in plasmas and correlation with measured etch characteristics of silicon dioxide. Plasma Sources Sci Technol 5(2):200
11. Li X, Ling L, Hua X et al (2003) Effects of Ar and O_2 additives on SiO_2 etching in C_4F_8-based plasmas. J Vac Sci Technol A 21(1):284–293
12. Li X, Ling L, Hua X et al (2003) Characteristics of C_4F_8 plasmas with Ar, Ne, and He additives for SiO_2 etching in an inductively coupled plasma (ICP) reactor. J Vac Sci Technol A 21(6):1955–1963
13. Matsui M, Tatsumi T, Sekine M (2001) Relationship of etch reaction and reactive species flux in C_4F_8/Ar/O_2 plasma for SiO_2 selective etching over Si and Si_3N_4. J Vac Sci Technol A 19(5):2089–2096
14. Sankaran A, Kushner MJ (2005) Etching of porous and solid SiO_2in Ar/c-C_4F_8, O_2/c-C_4F_8 and Ar/O_2/c-C_4F_8 plasmas. J Appl Phys 97(2):023307
15. Standaert TEFM, Hedlund C, Joseph EA et al (2004) Role of fluorocarbon film formation in the etching of silicon, silicon dioxide, silicon nitride, and amorphous hydrogenated silicon carbide. J Vac Sci Technol A 22(1):53–60
16. Chun I, Efremov A, Yeom GY, Kwon KH (2015) A comparative study of CF_4/O2/Ar and C_4F_8/O_2/Ar plasmas for dry etching applications. Thin Solid Films 579:136–143
17. Lee J, Efremov A, Yeom GY et al (2015) Application of Si and SiO_2 etching mechanisms in CF_4/C_4F_8/Ar inductively coupled plasmas for nanoscale patterns. J Nanosci Nanotechno 15(10):8340–8347
18. Lim N, Efremov A, Kwon KH (2019) Gas-phase chemistry and etching mechanism of SiNx thin films in C_4F_8 + Ar inductively coupled plasma. Thin Solid Films 685:97–107
19. Sasaki K, Kawai Y, Kadota K (1999) Determination of fluorine atom density in reactive plasmas by vacuum ultraviolet absorption spectroscopy at 95.85 nm. Rev Sci Instrum 70(1):76–81
20. Kimura T, Noto M (2006) Experimental study and global model of inductively coupled CF_4/ O_2 discharges. J Appl Phys 100(6):063303
21. Plumb IC, Ryan KR (1986) A model of the chemical processes occurring in CF_4/O_2 discharges used in plasma etching. Plasma Chem Plasma Process 6(3):205–230
22. Efremov A, Lee J, Kim J (2017) On the control of plasma parameters and active species kinetics in CF4 + O2 + Ar gas mixture by CF4/O2 and O2/Ar mixing ratios. Plasma Chem Plasma Process 37(5):1445–1462
23. Shun'ko E (2008) Langmuir probe in theory and practice. Universal Publishers, Boca Raton
24. Kwon KH, Efremov A, Kim M et al (2010) A model-based analysis of plasma parameters and composition in HBr/X (X = Ar, He, N_2) inductively coupled plasmas. J Electrochem Soc 157(5):H574–H579
25. Hsu CC, Nierode MA, Coburn JW, Graves DB (2006) Comparison of model and experiment for Ar, Ar/O_2 and Ar/O_2/Cl_2 inductively coupled plasmas. J Phys D Appl Phys 39(15):3272
26. Lee BJ, Lee BJ, Efremov A et al (2016) Etching characteristics and mechanisms of MoS_2 2D Crystals in O_2/Ar inductively coupled plasma. J Nanosci Nanotechno 16(11):11201–11209

27. Bose D, Rauf S, Hash DB et al (2004) Monte Carlo sensitivity analysis of CF2 and CF radical densities in ac-C4F8 plasma. J Vac Sci Technol A 22(6):2290–2298
28. Font GI, Morgan WL, Mennenga G (2002) Cross-section set and chemistry model for the simulation of c-C_4F_8 plasma discharges. J Appl Phys 91(6):3530–3538
29. Gray DC, Tepermeister I, Sawin HH (1993) Phenomenological modeling of ion-enhanced surface kinetics in fluorine-based plasma etching. J Vac Sci Technol B 11(4):1243–1257
30. Winters HF, Coburn JW, Chuang TJ (1983) Surface processes in plasma-assisted etching environments. J Vac Sci Technol B 1(2):469–480
31. Coburn JW (1982) Plasma etching and reactive ion etching. AVS monograph series. AIP, New York
32. Stoffels WW, Stoffels E, Tachibana K (1998) Polymerization of fluorocarbons in reactive ion etching plasmas. J Vac Sci Technol A 16(1):87–95
33. Lee J, Kim J, Efremov A et al (2019) Etching mechanisms and surface conditions for SiO_xN_y thin films in $CF_4 + CHF_3 + O_2$ inductively coupled plasma. Plasma Chem Plasma Process 39(4):1127–1144
34. Schaepkens M, Standaert TEFM, Rueger NR et al (1999) Study of the SiO_2-to-Si_3N_4 etch selectivity mechanism in inductively coupled fluorocarbon plasmas and a comparison with the SiO_2-to-Si mechanism. J Vac Sci Technol A 17(1):26–37
35. Cunge G, Kogelschatz M, Joubert O, Sadeghi N (2005) Plasma-wall interactions during silicon etching processes in high-density HBr/Cl_2/O_2 plasmas. Plasma Sources Sci Technol 14:S42–S52
36. Kim DK, Kim YK, Lee H (2007) A study of the role of HBr and oxygen on the etch selectivity and the post-etch profile in a polysilicon/oxide etch using HBr/O_2 based high density plasma for advanced DRAMs. Mat Sci Semicon Proc 10(1):41–48